Recent Enhancements on Short-Fiber Reinforced Plastics Modeling in LS-DYNA

Christian Liebold[1], Andrea Erhart[1]

[1]DYNAmore GmbH, Stuttgart, Germany

1 Abstract

A two-scale constitutive model for short-fiber reinforced plastics is currently being realized in LS-DYNA associated with an appropriate data-mapper (DYNAmap). For reliable structural analysis of heterogeneous materials like SFRP, the anisotropic and locally varying effective elastic properties are determined through a homogenization process of the microstructure and provided for the structural analysis.
The complete process chain, from the manufacturing to the service conditions of the components can thus be simulated in connection as shown in Fig.1. The spatial varying information of fiber orientation and fiber content resulting from the injection molding simulation is transferred to the structural analysis model through DYNAmap. This mapper exports the appropriate information as `*INITIAL_STRESS_SOLID` cards to the structural analysis mesh. Using this information, homogenized anisotropic elastic material properties are determined and provided as material cards for standard anisotropic elastic material models or directly used for a structural analysis.
Chapter 2 deals with the corresponding data mapping, in chapter 3 the homogenization procedure is addressed.

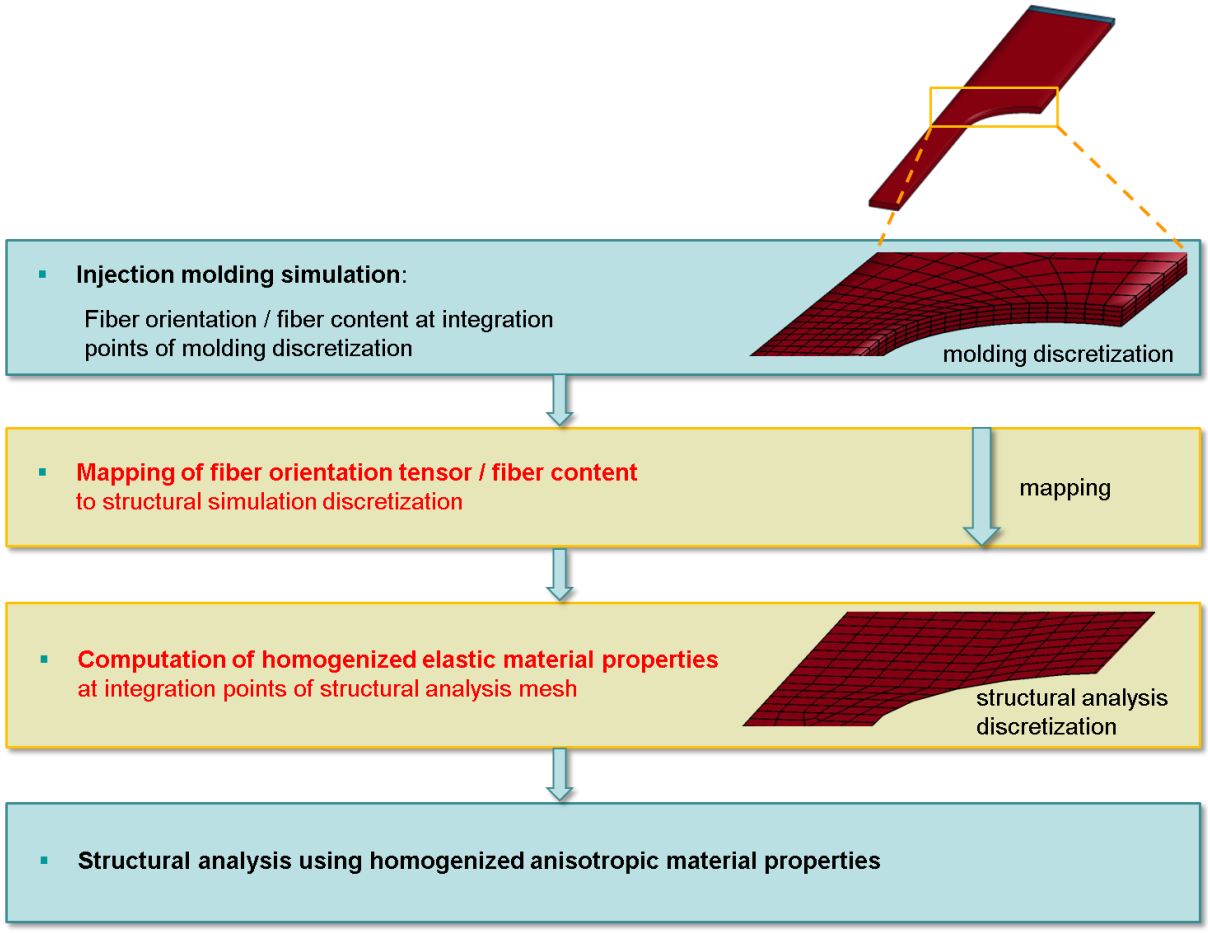

Fig.1: Overview over process chain "simulation of short fiber reinforced plastics": Process simulation, data mapping and structural analysis.

2 Data Mapping – DYNAmap

The development of a material model utilizing the results of infiltration simulation data goes in hand with the development of a proper data mapping procedure. Therefore, a new module called DYNAmap is introduced within this work which offers several possibilities to map simulation result data onto other meshes for further consideration within the following simulations along the process chain [15]. Several problems have to be considered when developing such a tool for infiltration simulations:

First of all, several software tools such as Moldflow® or Moldex3D® exist that provide simulation results in different data formats such as ascii, xml and many more which shall be readable for the mapping program. First developments take into account the Moldflow® xml-output data format.

Output data of infiltration simulations usually contain the fiber orientation tensor for each integration point considered within the simulation. As described below, this symmetric orientation tensor consists of six components, $\{a_{11}, a_{22}, a_{33}, a_{12}, a_{13}, a_{23}\}$ which can be sorted in a different order depending on the simulation software. An alternative output which is also widely used is the information about the direction of the first two eigenvectors (EV) together with the two corresponding eigenvalues of the mentioned orientation tensor. The third axis and the corresponding eigenvalue can be derived from the given eigenvectors and eigenvalues. It is important to consider which coordinate system is used for the direction dependent data output. Both, a global coordinate system as well as an element coordinate system which is given by the element's node numbering order are conceivable.

Usually, process simulations and the following crushing analysis are preformed within different unit systems. This has to be respected by the mapping tool since data might have to scaled properly to perform a correct closest point search and averaging. The unit systems within the different simulations can therefore be defined by the user. Furthermore, the coordinate systems being used within the different analysis might be different as well. Therefore, a mesh- and data transformation for the direction dependent values has to be realized.

The main focus has to be given towards the different discretizations being used within the different simulation models. A standard Moldflow® simulation usually takes up to 13 integration points (IP) through the element's thickness into account whereas crushing analysis usually consider only three to five IPs through the element's thickness. Besides that, process simulations in general do use a much smaller element size compared to durability analysis which has to be considered within the mapping and averaging procedures. Also, different element types are used, see Fig. 2.

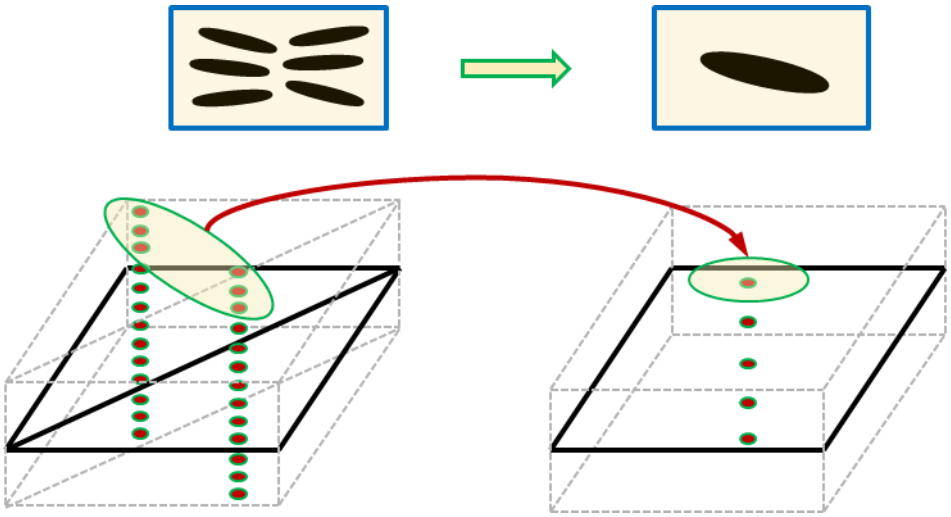

Fig.2: Orientation data mapping from 13 IPs through the element's thickness of triangular shell element's onto quadrilateral shell element's using five integration points over the thickness. A proper tensor averaging method has to be developed.

By now, the mapping algorithm is realized with a nearest neighbor search which maps the data without any further averaging, homogenization or a weighting approach. Approaches which might help

to improve the mapping of scalar and tensorial data are given in [17] and [18]. The main problem thereby is to consider the conservation of energy throughout the areas being mapped as well as to preserve shape and direction of the tensorial and therefor direction dependent data being transformed.

Nevertheless, the importance of a proper data mapping for short fiber reinforced plastics shall be illustrated in Fig. 3. The phenomena which can be observed when taking a look at the fiber orientations over the part's thickness is that the main fiber orientation of the outer layer's is completely opposite to the orientation which can be observed in the middle of the component. This fact increases the importance of a proper homogenization method, especially if a relatively low number of integration points is used through the thickness of the target mesh.

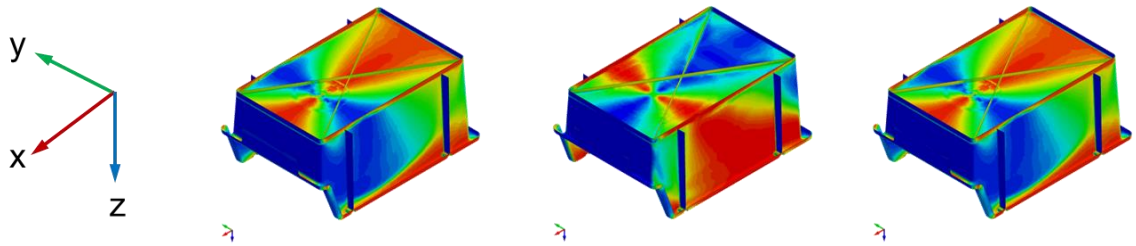

Fig.3: Visualization of the fiber orientation tensor component a_{11} which is parallel to the global x-direction. On the left, the component is displayed for the lower (-z) integration point, the figure in the middle shows the integration point in the middle of the storage box and on the right, the component is displayed for the upper (+z) integration point.

With the developed mapping program DYNAmap, the user can define the source and target meshes as well as an orientation file within a standardized ascii input file which will be read prior the actual mapping process starts. In case that a transformation from the source towards the target mesh is necessary, this will be performed before the mapping, too. By now, the user can define the number of target layers and the orientation tensor data will be mapped and initialized within the material model using `*INITIAL_STRESS_SHELL` or `*_SOLID` cards. An additional flag which can switch between the output of globally or locally oriented tensor data will be implemented soon.

3 Realized homogenization procedure for short fiber reinforced materials

One reasonable strategy to determine homogenized equivalent elastic properties of non-aligned short-fiber reinforced composites, depending on the fiber volume fraction and fiber orientation distribution, is, to carry out a two-step process as visualized in Fig. 3 and described in Advani & Tucker [1], Mlekusch [7] or Dray et al. [2]:

In a first step, homogenized properties of a *pseudo-composite* with *aligned (unidirectional)* fiber-reinforcement, however with appropriate fiber geometry, content and fiber and matrix elastic properties are determined by analytical homogenization methods, for example based on Eshelbys equivalent inclusion method [4] combined with Mori & Tanakas double inhomogeneity model [9]. For an overview on analytical homogenization estimates, we refer to Dvorak [3].

As second step, an orientation averaging is performed, i.e. the fact, that we are not dealing with aligned fibers, but with spatial varying fiber orientation distribution, is taken into account.

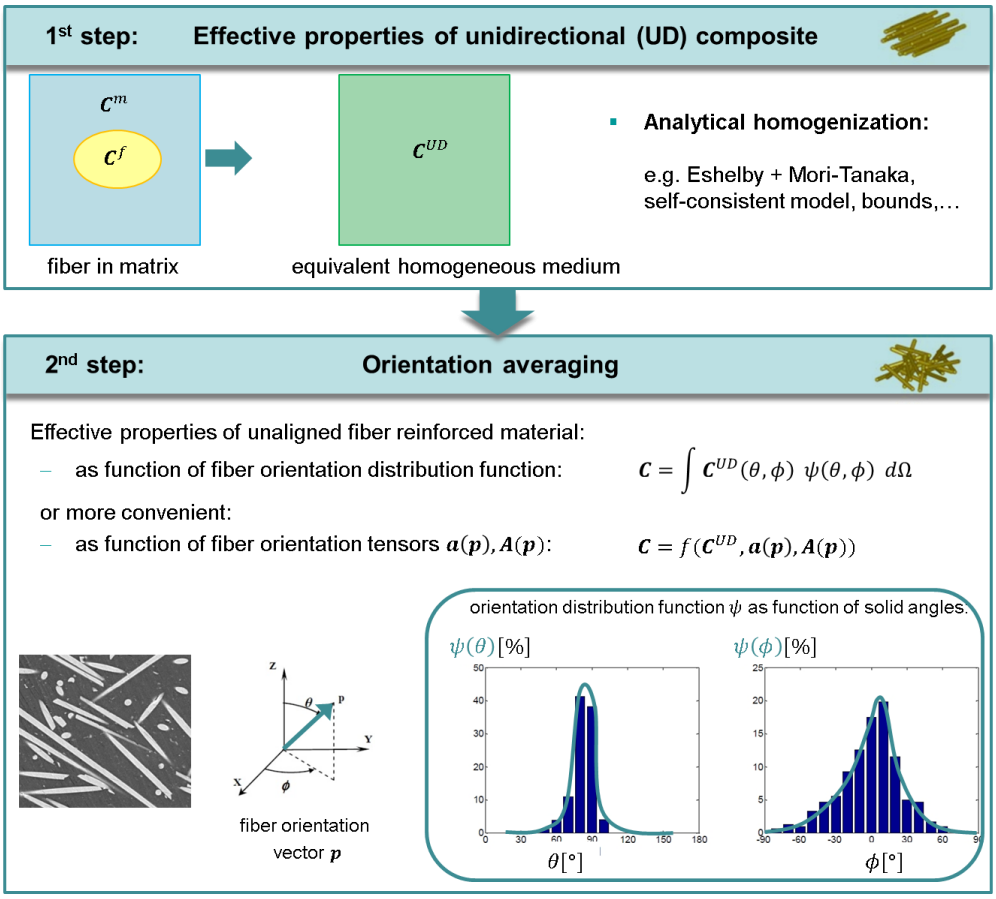

Fig.4: Two-step homogenization process for SFRP

3.1 1st step: Homogenized properties of aligned (unidirectional) fiber-reinforced composite

For aligned fiber-reinforced composites there exists a multitude of analytical homogenization models, in order to approximate the effective elastic properties. Very popular are the semi-empirical Halpin-Tsai-equations (see [5]), derived from the self-consistent method, applicable for both isotropic and transversal isotropic fibers. Another very common model was developed by Tandon & Weng [13]. It can be used not only for fiber reinforced composites but as well for heterogeneous materials with spherical, ellipsoidal or disk-shaped inclusions. This formulation is based on Eshelby [4] and Mori & Tanaka [9] and developed for higher fiber content.
At the moment, the Halpin-Tsai equations, the Tandon-Weng-Model and the rule of mixtures, see for example Lusti [6], have been implemented.

3.1.1 Example: Glass-fibers in thermoplastic matrix material

Exemplarily, the effective properties of a glass-fiber reinforced thermoplast are estimated, using the Halpin-Tsai-equations. To have a checkup, material properties of isotropic fibers and isotropic matrix material, as well as fiber content of 20.0 vol % and fiber aspect ratio=100.0 of an application published by Advani & Tucker [1] have been used, see Table 1.

E_f	ν_f	E_m	ν_m
72400 MPa	0.2	3400 MPa	0.35

Table 1: Elastic constants for glass fibers and matrix material, given by Advani & Tucker [1].

With x_1 being the fiber orientation, this results in following transversal isotropic elastic effective constants for the unidirectional composite, see Table 2.

	E_1	$E_2 = E_3$	$G_{12} = G_{13}$	G_{23}	ν_{12}
LS-DYNA	16220 MPa	5620 MPa	1850 MPa	1750 MPa	0.32
Advani&Tucker	16221 MPa	5621 MPa	1848 MPa	1745 MPa	0.32

Table 2: Effective transversal isotropic elastic constants of composite.

3.2 2nd step: Orientation averaging

After determining the effective material properties $\boldsymbol{C}^{UD}$ of the corresponding *unidirectional* reinforced material, it is necessary for an accurate prediction of the effective anisotropic material properties $\boldsymbol{C}$ of non-aligned short fiber reinforced composites, to take the pointwise fiber orientation distribution into account.
This could be done very plausible by means of an integral of the unidirectional elasticity tensor $\boldsymbol{C}^{UD}$ weighted with the orientation distribution function $\psi(\phi, \theta)$ over the solid angels ϕ and θ:

$$\boldsymbol{C} = \int \boldsymbol{C}^{UD}(\theta, \phi)\ \psi(\theta, \phi)\ d\Omega. \tag{1}$$

Hereby the orientation distribution function ψ describes the probability, to have fibers in the direction defined by ϕ and θ.
But for most cases the orientation distributions function is not available; furthermore, the numerical evaluation of this integral is impractical.
A more convenient and popular alternative to conduct the orientation averaging is, to use a tensorial description of the fiber orientation, as described by Advani & Tucker [1]. To this end, the fiber orientation vector $\boldsymbol{p} = \langle sin\theta\ cos\psi, sin\theta\ sin\psi, \cos\theta \rangle^T$ is introduced, see Fig. 3.

The orientation state of fibers can be reflected by a truncated series of even order orientation tensors, see Advani & Tucker [1] for details. For the evaluation of the effective 4th order elasticity tensor $\boldsymbol{C}$, the 2nd and the 4th order orientation tensor are needed. They are given by:

$$a_{ij} = \int p_i p_j\ \psi(\theta, \phi)\ d\Omega \quad \text{and} \quad A_{ijkl} = \int p_i p_j p_k p_l\ \psi(\theta, \phi)\ d\Omega. \tag{2}$$

The resulting equations, to evaluate the effective anisotropic elasticity tensor $\boldsymbol{C}$ are given by Advani & Tucker [1] as follows; x_1 is hereby the fiber direction of the unidirectional elasticity tensor C^{UD}.

$$\boldsymbol{C} = \int \boldsymbol{C}^{UD}(\theta, \phi)\ \psi(\theta, \phi)\ d\Omega \tag{3}$$

$$C_{ijkl} = B_1 A_{ijkl} + B_2\left(a_{ij}\delta_{kl} + a_{kl}\delta_{ij}\right) + B_3\left(a_{ik}\delta_{jl} + a_{il}\delta_{jk} + a_{jl}\delta_{ik} + a_{jk}\delta_{il}\right) + B_4\left(\delta_{ij}\delta_{kl}\right) + B_5\left(\delta_{ik}\delta_{jl} + \delta_{il}\delta_{jk}\right)$$

$$B_1 = C^{UD}{}_{1111} + C^{UD}{}_{2222} - 2C^{UD}{}_{1122} - 4CC^{UD}{}_{1212} \tag{4}$$

$$B_2 = C^{UD}{}_{1122} + C^{UD}{}_{2233} \tag{5}$$

$$B_3 = C^{UD}{}_{1212} + {}^1/_2\,(C^{UD}{}_{2233} - C^{UD}{}_{2222}) \tag{6}$$

$$B_4 = C^{UD}{}_{2233} \tag{7}$$

$$B_5 = {}^1/_2\,(C^{UD}{}_{2222} - C^{UD}{}_{2233}) \tag{8}$$

For most applications, the 2nd order orientation tensor $\boldsymbol{a}$ is available as a result of a manufacturing simulation, whereas the 4th order orientation tensor $\boldsymbol{A}$ is usually unknown.
Therefore a so called *closure approximation* for estimating the 4th order orientation tensor has to be performed. Various assumptions for determining closure approximations are given in the literature and a comparison of their accuracy is for example given in Dray et al. [2].

3.2.1 Closure approximation

At the moment, the linear, the quadratic and the hybrid closure approximation have been implemented. Further approximations will be realized in the near future.

- Linear closure approximation:

$$A^L{}_{ijkl} = -\frac{1}{35}\left(\delta_{ij}\delta_{kl} + \delta_{ik}\delta_{jl} + \delta_{il}\delta_{jk}\right) + \frac{1}{7}\left(a_{ij}\delta_{kl} + a_{ik}\delta_{jl} + a_{il}\delta_{jk} + a_{kl}\delta_{ij} + a_{jl}\delta_{ik} + a_{jk}\delta_{il}\right). \quad (8)$$

The linear closure approximation is exact for a complete isotropic fiber orientation.

- Quadratic closure approximation:

$$A^Q{}_{ijkl} = a_{ij}a_{kl}. \quad (9)$$

The quadratic closure approximation is exact for complete aligned fibers.

- Hybrid closure approximation:

$$A^H{}_{ijkl} = (1-f)A^L{}_{ijkl} + fA^Q{}_{ijkl}\,. \quad (10)$$

The hybrid closure approximation is a mixture of the linear and quadratic closure approximations. In average, the hybrid closure approximation is more accurate than linear or quadratic closures, because the linear one is accurate for nearly randomly fiber distribution and the quadratic one is accurate for nearly aligned fiber distribution. The scalar factor f can be defined as a function of the 2nd order orientation tensor:

$$f = \frac{3}{2}a_{ij}a_{ij} - \frac{1}{2} \quad \text{or alternatively} \quad f = 1 - 27\,det(a_{ij}). \quad (11)$$

3.2.2 Application example

In their paper, Dray et al. [2] provide experimental results of a polyacrylamide matrix (density=2.6E-09 t/mm^3) reinforced with 16.5 vol% glass fibers (density=1.2E-09 t/mm^3) with an aspect ratio of 30.0, both constituents are assumed to be isotropic, the material properties are given in Table 3.

E_f	ν_f	E_m	ν_m
74000.0 MPa	0.25	5100.0 MPa	0.395

Table 3: Elastic properties of glass fibers and matrix material (Dray et al. [2]).

Dray et al. [2] measured the fiber orientation tensor 2nd order by analyzing series of images obtained with a scanning electron microscope,

$$\boldsymbol{a} = \begin{bmatrix} 0.793 & 0.016 & 0.053 \\ 0.016 & 0.179 & 0.006 \\ 0.053 & 0.006 & 0.028 \end{bmatrix},$$

as well as the Youngs moduli along the injection flow (E_1) and the transverse direction (E_2). In Table 4, homogenization results with LS-DYNA using the Halpin-Tsai-equations for the unidirectional composite, in combination with either linear, or quadratic or hybrid closure approximations of the 4th order fiber orientation tensor $\boldsymbol{A}$ as well as the experimental results of Dray et al [2] are given, displaying a nice accordance.

	E_1	$E_2 = E_3$
LS-DYNA, Halpin-Tsai, linear closure approximation	11600 MPa	7900 MPa
LS-DYNA, Halpin-Tsai, quadratic closure approximation	11400 MPa	7230 MPa

LS-DYNA, Halpin-Tsai, hybrid closure approximation	11500 MPa	7300 MPa
Dray et al. [2], experimental results	11800 MPa	7220 MPa

Table 4: Youngs moduli in injection flow and transverse direction measured by Dray et al. [2] in comparison to simulation results.

4 Numerical application: Stackable storage box

Following application example of an injection molded stackable box under impact loading is taken from Jennrich et al. [14]. Thanks to Mr. Weber and Mr. Kolling for kindly allowing us, to use the geometry and the injection molding simulation results as the fiber orientation (see Fig.4 left) which has been transmitted to the structural analysis model via DYNA-map. For the constituents fiber and matrix, we assumed isotropic elastic behavior and material properties given in Table 5, with a fiber volume fraction of 0.165 and an aspect ratio of 25.0.

E_f	ν_f	ρ_f	E_m	ν_m	ρ_m
74000.0 MPa	0.25	2.6 E-09 t/mm^3	5100.0 MPa	0.35	1.2E-09 t/mm^3

Table 5: Elastic properties of glass fibers and matrix material.

The spherical impactor has a diameter of 19.6 mm, a mass of 0.0052t, is assumed to be rigid and impacts with an initial velocity of 1000 mm/s.

The homogenization was performed using the Halpin-Tsai-equations and the linear closure approximation. In Fig. 4, the 11-componente of the fiber orientation tensor in the mid plane of the specimen is depicted on the left, a result of the injection molding simulation transferred to the model using the data-mapper. On the right the special distribution of the 1111-component of the homogenized elasticity tensor in the mid plane of the specimen is shown. The obvious similarity of the special distribution illustrates, how the elasticity tensor reflects the fiber orientation distribution.

Fiber orientation tensor component a_{11}:

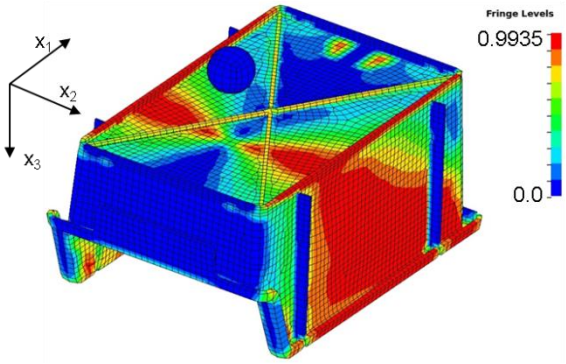

Elasticity tensor component C_{1111} of homogenized equivalent medium:

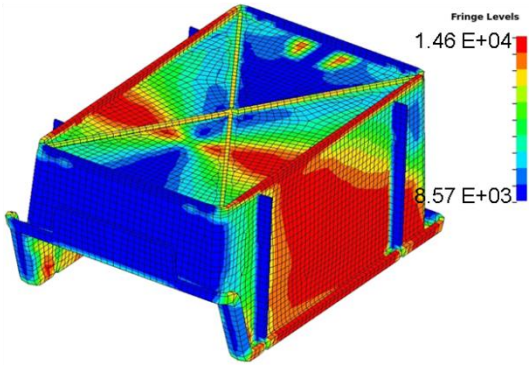

Fig.5: Component a_{11} of 2nd order fiber orientation tensor (left); elasticity tensor component C_{1111} of homogenized equivalent medium (right). Both: In the mid plane of the specimen.

In Fig.5 the system response as the deflection under the impactor (left) and the contact force (right) over the time is diagrammed. The red curve (A) is for the case of pure matrix material, curve B in green is the system response of the fiber reinforced composite material. Due to the reinforcement, the deflection is much smaller (curve B, left) than for the pure matrix material (curve A, left), while the contact force is larger for the reinforced composite (curve B, right) than for the pure matrix material (curve A, right).

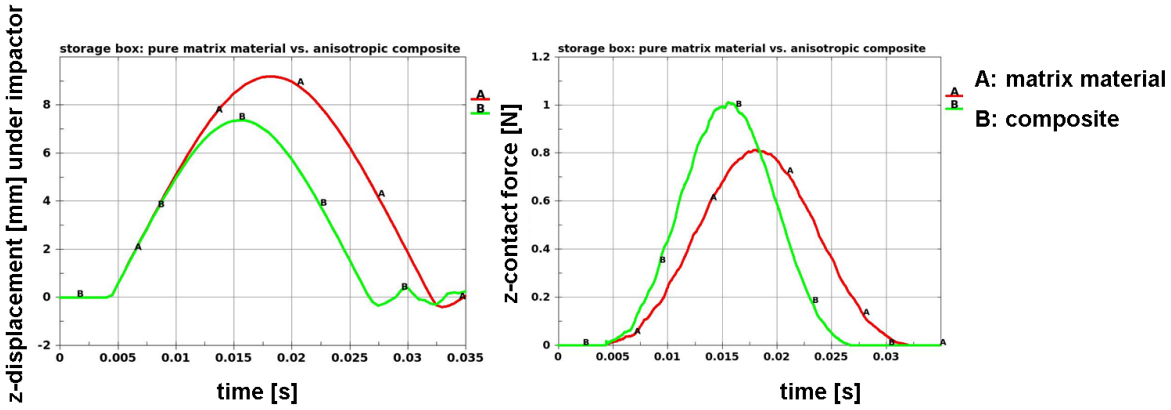

Fig.6: left: z-displacement vs. time under the impactor. Right: Contact force vs. time. Comparison of system responses: pure matrix material (red) vs. fiber reinforced composite (green).

In Fig.6 the vertical displacement distribution at the moment of maximum deflection (t=0.016 s) is given, on the left for the pure matrix material, on the right for the fiber reinforced composite.

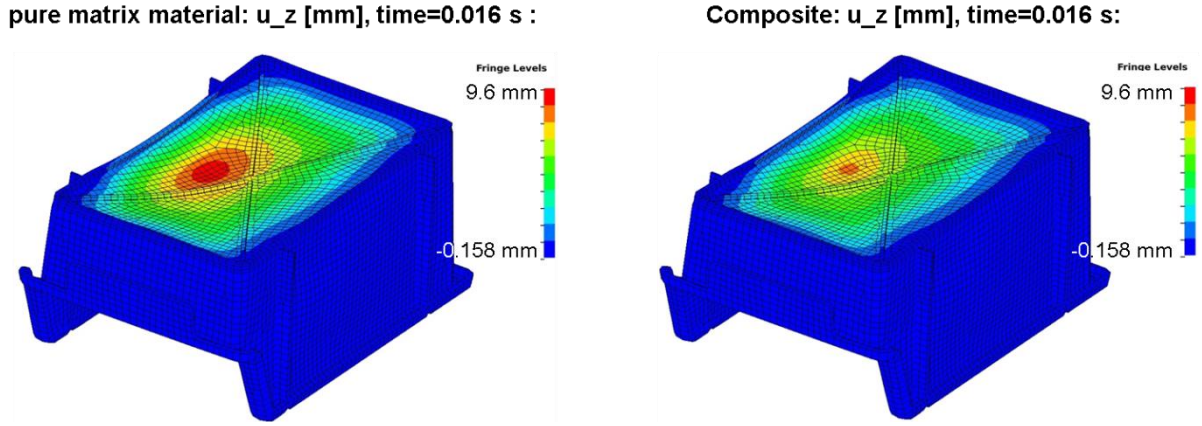

Fig.7: Comparison system responses: z-displacement at t=0.016 s of pure matrix material (left) vs. fiber reinforced composite (right).

5 Summary

Within this paper, the formulation of a two-scale anisotropic elastic material model for short fiber reinforced materials in combination with DYNA-map is described and a first application example from the molding simulation to a serviceability test simulation as a closed process chain was presented.

6 Acknowledgements

This work has been promoted by the BMWI (Bundesministerium für Wirtschaft und Energie) within the project “SWIM-RTM”. We would like to thank Mr. Gerhard Weber, Mr. Stefan Kolling and Co-workers for kindly allowing us, to utilize their molding simulation results of the storage box application.

7 Literature

[1] Advani, S. G., Tucker, C. L., Journal of Rheology, The Use of Tensors to Describe and Predict Fiber Orientation in Short Fiber Composites, 31 (8), 1987, 751-784.

[2] Dray, D., Gilormini, P., Regnier, G., Composites Science and Technology, Elsevier, Comparison of several closure approximations for evaluating the thermoelastic properties of an injection molded short-fiber composite, 2007, 1601-1610.

[3] Dvorak, G., Micromechanics of Composite Materials, Springer Heidelberg, 2013.

[4] Eshelby J. D., Proc. R. Soc. Lond., The determination of the elastic field of an ellipsoidal inclusion, and related problems. A241, 1957, 376-396.

[5] Halpin, J. C., Kardos, J. L.., Polym. Eng. Sci., The Halpin-Tsai Equations: A Review, 16, 1978, 344-352.

[6] Lusti, H. R., Property Predictions for Short Fiber and Platelet Filled Materials by Finite Element Calculations, PhD-thesis, Swiss Federal Institute of Technology - ETH Zürich, 2003.

[7] Mlekusch, B., Kurzfaserverstärkte Thermoplaste Charakterisierung und Messung der Faserorientierung, thermoelastische Eigenschaften sowie Schwinden und Verzug, PhD-thesis, Institut für Konstruieren mit Kunst- und Verbundstoffen - Montanuniversität Leoben, 1997.

[8] Mlekusch B., Comp. Sci. Technol., Thermoelastic properties of short-fibre-reinforced thermoplastics, 59, 1999, 911-923.

[9] Mori, T., Tanaka, K., Acta Metallurgica, Average Stress in Matrix and Average elastic Energy of Materials with misfitting Inclusions, 21, 1973, 571-574.

[10] Mura, T. Micromechanics of defects in solids, Martinus Nijhoff Publishers, Boston, 1987.

[11] Pierard, Friebel, Doghri, I., Composites Science and Technology, Mean-field homogenization of multi-phase thermo-elastic composites: a general framework and its validation, 64, 2004, 1587–1603.

[12] Radtke, A., Steifigkeitsberechnung von diskontinuierlich faserverstärkten Thermoplasten auf der Basis von Faserorientierungs- und Faserlängenverteilungen, PhD-thesis, Institut für Kunststoffprüfung und Kunststoffkunde, Universität Stuttgart, 2009.

[13] Tandon G. P., Weng G. J., Comp. Sci. Technol., Average stress in the matrix and effective moduli of randomly oriented composites, 27, 1986, 111-132.

[14] Jennrich, R., Roth, M., Kolling, S., Liebold, C., Weber, G., Experimental and Numerical Analysis of a Glass Fiber Reinforced Plastic, 13. LS-DYNA Forum, Bamberg, 2014.

[15] Liebold, C., DYNAmap User's manual, DYNAmore GmbH, Stuttgart, 2015.

[16] Livermore Software Technology Corporation (LSTC), LS-DYNA User's Manual, Vol. I, Livermore, CA, 2015.

[17] Shepard, D., A two-dimensional interpolation function for irregularly-spaced data, Proceeding ACM National Conference, 1968.

[18] Gahm, J. K., Microstructural Feature-based Processing and Analysis of Diffusion Tensor MRI, PhD Thesis, University of California, USA, 2014.